Chapter 4

P3DDT Peak Profile Analysis

4.1 Introduction

The increasing molecular level complexity of polymeric materials, in the pursuit of specific nanoscale architectures, has created a vastly expanding litany of possible structural forms possessing a wealth of subtle, contradictory and often interrelated structural characteristics. In addition to the overall organization of the fundamental base structure, these systems can also exhibit pronounced microscopic inhomogeneities indicative of paracrystalinity, structural defects, and systematic disorder. These latter effects are also intimately related to the molecular design and necessarily play an integral part in defining a material's limitations.

Hosemann proposed that polymers and other materials exist in the solid state as something different from perfect crystals [36,110–112]. Instead of describing a solid as being composed of a 3D crystalline lattice with statistical variations form these equilibrium positions, a better description may be one in which lattice cells exist as distorted parallelograms that are still ordered in rows and columns. The lattices of these "paracrystals" have distance statistics which can be calculated by means of a convolution polynomial. Some examples of paracrystal order are given in Ref. [36].

The well-defined lamellar construction present in PATs is paralleled by a number of scattering attributes indicative of local disorder and strong structural heterogeneities which likely include paracrystalinity. These irregularities may be intrinsic (the presence of gauche conformers and side chain disorder) or extrinsic (the extent of regioregularity of the side chain anchoring). Imperfect materials often exhibit systematic effects in the Bragg scattering profiles which can be quantified through a detailed lineshape analysis.

Traditional lineshape analysis observes that peak shapes are the result of a convolution of various broadening mechanisms: a distribution of finite crystal sizes, variation in lattice parameters from crystal to crystal, and displacement disorder within a crystal. The effects of crystal size are independent of the order for a given series of reflections, while lattice parameter fluctuation and displacement disorder have a functional dependence with respect to the order for a given set of reflections.

For materials whose x-ray diffraction profiles exhibit multiple orders of a given reflection, the effects of crystal size and disorder can, in principle, be unambiguously separated. In practice, however, the problematical nature of polymer diffraction profiles often makes this separation a nontrivial exercise. This technique has traditionally been applied to metals having undergone mechanical deformations [113–115,50], but is has also been applied to a small number of polymer systems with limited success [116–118]. Difficulties with determining the correct, noncrystalline background, and a pronounced lack of multiple diffraction peak orders are the primary reasons why few have attempted applying this methodology to polymer systems.

P3DDT is a polymer host that does contain extensive local disorder, and the presence of five (or more) distinguishable $(h00)$ orders of reflection make it an attractive model candidate for a rigorous separation of size and disorder effects.

The semicrystalline nature of P3DDT has been studied quite extensively, as detailed in the last chapter. Moreover, the (100) reflections, and to a varied extent the other ($h00$) reflections indicative of the lamellar d-spacing in this material, narrow considerably during heating through the LC transition, with an associated increase of 15% in crystal size (in the temperature range of 10°C to 120°C) as determined by the method of Debye-Scherrer from x-ray diffraction line profiles [89,102].

Additionally, the thermotropic evolution of the P3AT molecule is qualitatively understood. The longer side chain P3ATs, including P3DDT, have been analyzed by a variety of techniques including UV absorption, differential calorimetry (DSC), Fourier transform infrared (FTIR), and x-ray diffraction [89,93,95,102]. These studies are consistent with P3DDT molecules, at temperatures below 25°C, having a well defined lamellar structure (see last chapter) where both the skeletal backbone, and the alkyl side groups have almost fully extended *trans* conformations. The side chains are strongly tilted at an angle such that the side chain nesting approximates a 4.5Å hexagonal close-packing in close correspondence to the average packing of pure alkanes or polyethylene [108]. A secondary crystalline ordering of the side chains is contained in the methylenes farthest from the backbone. P3ATs with side chains of octyl and shorter do not show this side chain crystalization. This is evident from DSC and x-ray diffraction studies of P3ATs with various lengths of side chains. Other studies of side chain substituted polymers support a model with side chain crystallinity beginning around the 10^{th} methylene group [119].

DSC studies reveal that P3DDT has two broad endothermic peaks at ~32°C and ~56°C and melts completely around 130°C [95]. The 30°C peak has been attributed,by some, to the melting of the side chain crystallinity, while the 60°C transition is liquid crystalline (LC) in nature, whereby the "out-of-phase" [see next chapter Fig. 5.53(b)] staggering of neighboring P3AT chains is lost, creating a nematic, free floating, intrastack ordering. X-ray diffraction observes this transition through a loss in scattering intensity from the (002) meridional peak indicative of the interthiophene repeat [89]. The melting of the side chains must help enable this free floating LC phase behavior.

The following chapter, will review line profile analysis theory and methodology, as well as apply this method to the $(h00)$ reflections observed in a stretch oriented IR-P3DDT sample as a function of temperature, thereby investigating the disordering mechanisms in P3DDT in a direction perpendicular to both the polythiophene polymer axis and along the alkyl side chain direction, in effect studying side chain disorder. It will be shown that the observed narrowing of $(h00)$ diffraction profiles is not primarily associated with an increase in the crystal size effects. Although, an initial reduction of peak width on heating may be accompanied by an increase in crystal size, further narrowing is overwhelmingly associated with a singular and systematic reduction in the lattice parameter fluctuation, and an initial increase in disorder fluctuations near and around the LC transition temperature.

4.2 Lineshape Broadening Theory

In the absence of the instrumental contributions, the observed diffraction profiles are assumed to be representative of a convolution of three nominally independent broadening mechanisms: the crystallite coherence length (i.e., crystal size), and "long range" disorder including lattice parameter fluctuation, and displacement disorder (of the second kind). Each of these attributes yields a different order dependent functionality and, in the presence of at least two or more orders of reflection, can be uniquely specified. The exact microscopic origin of the latter two displacement fluctuations are varied and have been the subject of discussion but, for the purposes of this analysis, are not initially defined in any overt fashion. The actual process of deconvolution is further complicated by moments in the distribution which give rise to pseudo-Voigt lineshapes. While cumbersome these effects can be partially resolved using the general methods of Warren and Averbach [50,113–115], and more specifically the methodology utilized by Crist and Howard on polyethylene [118].

Displacement disorder of the first kind can be characterized as displacement defects or physical defects that disturb the "short range" order within a crystallite. This type of disorder manifests itself as thermal vibrations, frozen displacements or strains, vacancies, dislocations, etc., and does not effect the shape of a Bragg diffraction peak, but does influence the intensity in a manner consistent with that described by the Debye-Waller term used to model thermal vibration in structure factor modeling calculations [see equation (2.9)].

A prerequisite to performing a lineshape broadening analysis is that line profiles must first be corrected for all effects not reflective of the internal structure of the material. Scattering data must be corrected for all experimental effects including instrumental broadening, Lorentz-polarization effects, variations in atomic scattering, absorption, etc.. Once these factors have been taken into account, the n^{th} Fourier cosine transform coefficient of a h^{st} order diffraction peak is of the form [113,118,120,121]:

$$A_h(n) = A^S(n) \cdot A^e_h(n) \cdot A^D_h(n). \tag{4.13}$$

$$C_h(n) = \frac{1}{N} \sum_{j=N/2}^{N/2} I_j e^{\imath 2\pi n j/N} \tag{4.14}$$

$$L(n) = \frac{n}{N \Delta q} \tag{4.15}$$

where $A^S(n)$, $A^e_h(n)$, $A^D_h(n)$ are the normalized ($A_h(0) \equiv 1$) Fourier cosine coefficients for respectively, the crystallite size, lattice parameter fluctuation and displacement disorder. The Fourier coefficients with $n = -N/2, -N/2 + 1, ..., N/2$ contain information on a length scale $L(n)$ which is dependent on both the density, Δq, and number of scattering data points, N, considered for a given peak described by intensities I_j.

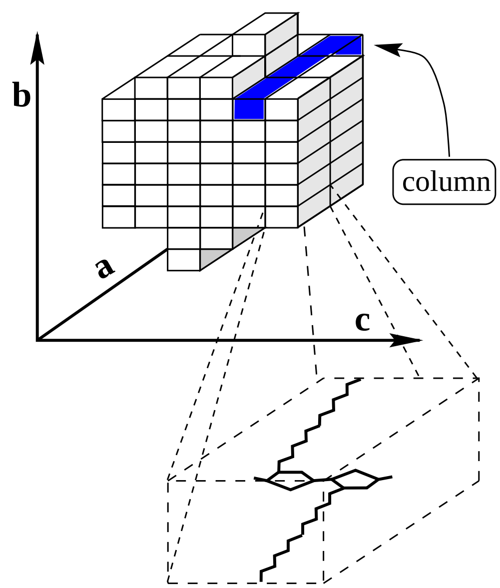

Figure 4.39: The representation of a crystal by considering it as being composed of *columns* of unit cells parallel to the a-axis.

The line broadening problem is traditionally constructed by considering an arbitrary distribution of crystallites, whereby each crystallite can be represented in terms of a 2D array of columns of unit cells along some $\vec{a}$ direction (see Fig. 4.39) [50]. The statistical description of the various broadening mechanisms is straight forward and is throughly discussed by Crist and Howard in Ref. [118]. The lattice parameter $d = |\vec{a}|$, defining the average lattice spacing within a particular crystallite, and $< d >$ defining the average lattice parameter value averaged over all crystallites, allows for the defining of the lattice parameter fluctuation reduced variance as $< e^2 >= (< d^2 > - < d >^2)/ < d >^2$. Likewise, Z_n describes the displacement between two unit cells within a column, n unit cells apart, having an ideal separation of nd and an actual separation of nd'. Takahashi [120] has argued that strain distributions with identical particles and independent displacements of unit cells can be regarded as the sum of a finite number of random variables with the following relation expected:

$$< Z_n^2 >= n < Z_1^2 >= n(< d'^2 > - < d >^2)/ < d >^2= ng^2. \tag{4.16}$$

The linear dependence of $< Z_n^2 >$ on n can be shown to result form various types of displacement disorder of the second kind [49,120,122,123]. The fact that the reduced positional uncertainty increases with separation is the signature of this type of disorder. The normalized Fourier cosine coefficients should then be of the following form [50]:

$$A_S(n) = N(n)/N_3 \tag{4.17}$$

$$A_h^e(n) = < \cos(2\pi hne) > \tag{4.18}$$

$$A_h^D(n) = < \cos(2\pi hZ_n) > \tag{4.19}$$

where $N(n)$ is the average number of crystal cells $L(n)$ apart per column of cells (each cell extends parallel to the layer normal direction $\vec{a}$), N_3 is the volume-averaged column length, or the effective average crystallite size. Equations (4.18) and (4.19) can be expanded with no loss of generality

$$A_h^e(n) = 1 - 2\pi^2h^2n^2e^2 + \mathcal{O}(4) - ... \tag{4.20}$$

$$\approx e^{-2\pi^2h^2e^2} \tag{4.21}$$

$$A_h^D(n) = 1 - 2\pi^2h^2 < Z_n^2 > +\mathcal{O}(4) - ... \tag{4.22}$$

$$\approx e^{-2\pi^2h^2<Z_n^2>} \tag{4.23}$$

with approximated equations (4.21) and (4.23) being valid for small fluctuations, or exact for fluctuations described by Gaussian statistics.

Following the method of Warren and Averbach [113,114], one can separate size and distortion effects by taking the natural logarithm of equation (4.13):

$$\ln A_h(n) = \ln N(n)/N_3 - 2\pi^2 h^2 n f(n) \tag{4.24}$$

$$f(n) = g^2 + n < e^2 > \tag{4.25}$$

Applying linear regression to the plot of $\ln A_l(n)$ vs h^2, while holding n constant, reveals the terms $\ln N(n)/N_3$ and $-2\pi^2 f(n)$ from the y-intercepts and slopes respectively. Thereafter, using the method of Crist and Howard [118], one can further separate the effects of lattice parameter and displacement disorder by a linear regression analysis of $f(n)$ verses n.

Errors in background determination and Fourier transformation, especially those resulting from the truncation of experimental diffraction peak tails, can lead to misrepresentation of the lowest order Fourier coefficients. Regrettably, these are the same coefficients that are the most accurately approximated by equations (4.21) and (4.23). These errors are evident when a plot of $\ln A_S(n)$ vs n possesses any negative curvature. This "hook effect" is not physically permittible since the volume weighted distribution of column lengths, $\mathrm{p}_v(\mathrm{n})$, is related to the second derivative of the crystal size coefficients, $\mathrm{A}_S(\mathrm{n})$, by the relation [124–127]

$$n\mathrm{p}_v(n) = \frac{d^2 A_S(n)}{dn^2}. \tag{4.26}$$

When the "hook effect" is present, the lowest order coefficients are generally ignored, and a linear fit of $f(n)$ verses n returns the values for $< e^2 >$ and $< g^2 >$.

When disorder fluctuations are not small, or when distributions do not exhibit Gaussian statistics, equations (4.21) and (4.23) may no longer be reliable approximations. This problem can be overcome with the availability of two or more orders of reflection, allowing for the implementation of the more general expansion

$$A_h(n) = \frac{N(n)}{N_3} \cdot [1 - \frac{4\pi^2 h^2 n}{2!}(g^2 + n < e^2 >) + \frac{16\pi^4 h^4 n^2}{4!}(g^4 + 2n < e^2 > g^2 + n^2 < e^4 >) - ...] \quad (4.27)$$

Alternatively, fitting $A_h(n)$ to $a_n - b_n h^2 + c_n h^4 - ...$ also allows for the separation of size and distortion effects from peak profiles [128].

4.3 Analysis Methodology

4.3.1 General Procedure

After iteratively unfolding the instrument profile from the diffraction spectra, as described in section 2.4.5, the data sets were corrected for Lorentz-polarization, absorption, variations in atomic scattering, and Debye-Waller effects [64]. Conversion from 2θ to wavevector, $q^{-1} = 2\sin\theta/\lambda$, was immediately followed by subtraction of an appropriate background. Each data set was fit with linear superposition of pseudo-Voigt peaks that approximated scattering by both "amorphous" and crystalline scattering features. To obtain a single peak lineshape, a composite of the "amorphous" background profile and all other fitted crystalline peaks was subtracted from the experimental data. Thus, the overlapping effect of neighboring diffraction peaks was accounted for by effectively treating them as a background features in extracting the particular peak profile of interest.

The "amorphous" background profile was consistent with backgrounds used in previous structure factor refinement studies [102] reported in the previous chapter. Three modest localized features, centered at 2θ values of 4.75°, 9.5°, and 14.2° (identified by arrows in the Fig. 4.41) have been attributed to the presence of a second crystalline phase and that has been seen highly regioregular P3AT samples [93]. The position of one of these two "background" peaks

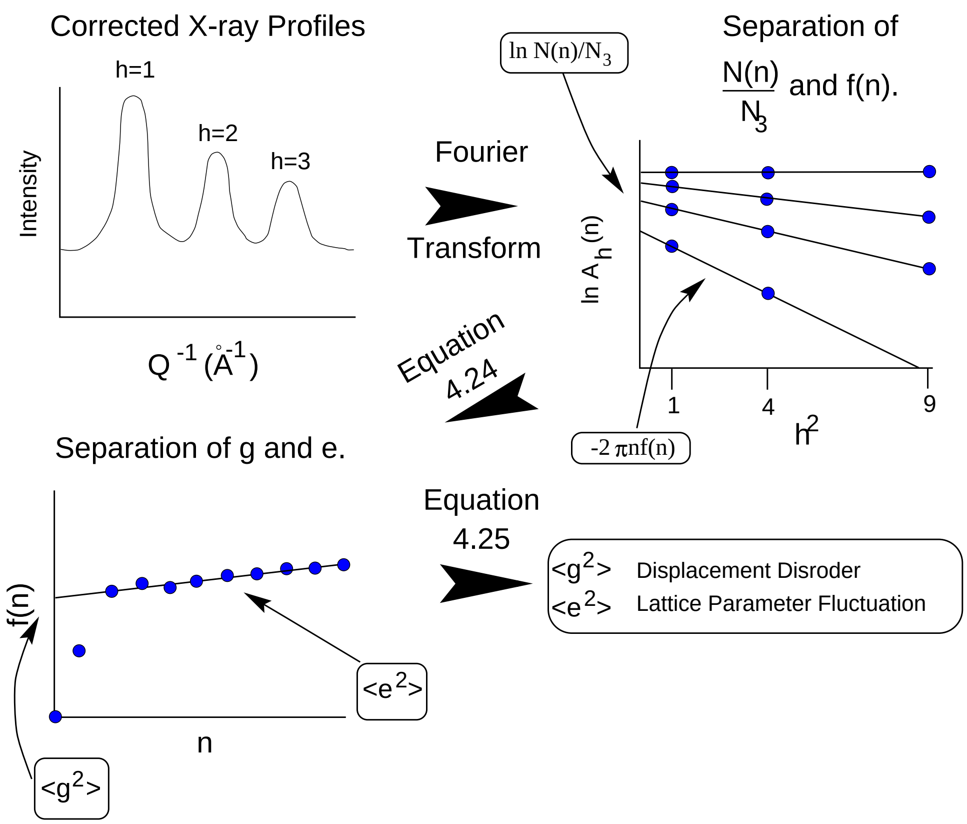

Figure 4.40: Schematic of peak profile analysis methodology.

resides very close to the 3^{rd} order reflection, making an unbiased determination of the shape of the (300) peak difficult at temperatures below the transition to the thermotropic LC phase (the type-II phase disappears at the higher temperatures). An additional experimental effect, arising from a combination of the broad character of the (h00) diffraction peaks, the large interlayer d-spacing and the associated small angle of the (100) reflection, produced an unavoidable "shadowing" of the beam stop over the low angle portion of the (100) peak, necessitating a correction for the (100) peak intensity at 2θ angles less than 3°.

A fast fourier transform (FFT) algorithm [129] was implemented to preform the necessary transforms. To minimize the introduction of truncation effects for the fourier coefficients of interest, tails were added to the resulting peak profiles [128]. Each peak was fit to a pseudo-Voigt lineshape and the tails from this function were added where data values approached zero to within the error of the data. All imaginary parts of the transform were negligible, but to insure that the above manipulations of the various diffraction profiles had not resulted in an unphysical peak shape (assuming mirror symmetry of the peaks), the real part of the transforms was inverse transformed and subtracted from the original data, revealing the "true" background used in this analysis. The resulting transforms were then fit by both equations (4.24) and (4.27) yielding numerical values for the aforementioned broadening parameters.

4.3.2 Discussion

Peak broadening theory, as an analytical tool applied to polymer diffraction patterns, has been sparsely applied, and with the advent of modern computing technology, this computationally demanding analysis has become much more accessible, yet only a single study of this type has been reported since the mid-late eighties [118]. An optimal system for study contains numerous orders of a given reflection that reside on either a flat or non-existent background. The narrower the diffraction peaks, the less ambiguous it becomes to account for background elimination, and the less important the previous requirement becomes. Most polymer spectra fail all of these criteria, and the few systems that do exhibit more than one or two orders of a reflection contain both a significant, non-trivial background and broad peak character. These complications have no doubt contributed to the anemic application of this analytical technique.

In order for an analysis of this type to be successful, an accurate account of "non-crystalline" scattering must be made. Some studies have used materials

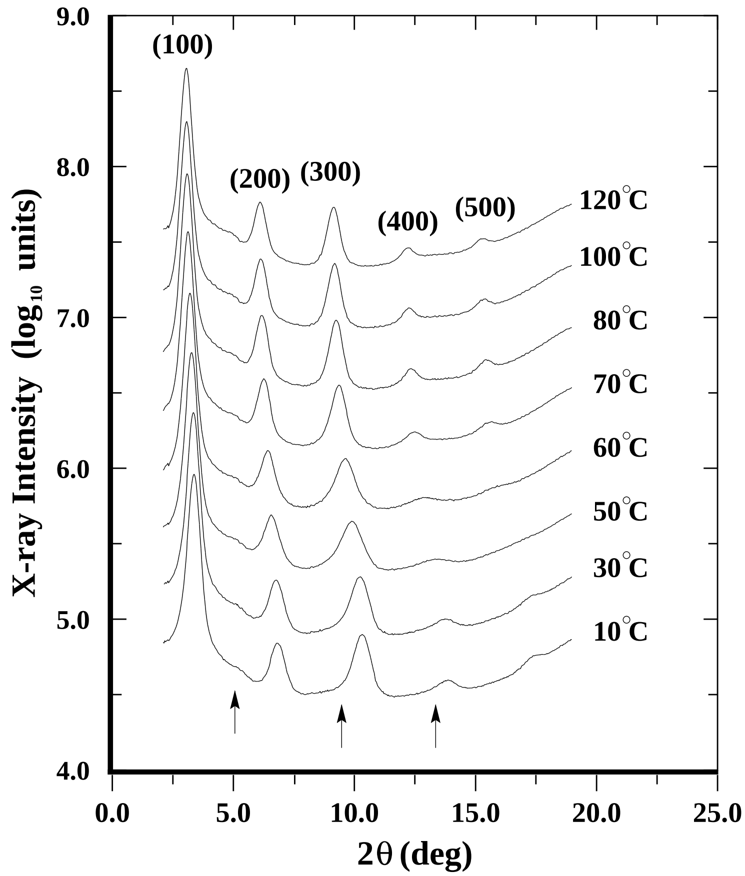

Figure 4.41: Plot of equatorial P3DDT scattering data showing the relative intensity variation for the first five ($h00$) orders of the interlayer repeat. Arrows indicate type-II background (see text).

quenched from a melt as a background for subsequent line shape analysis. The usefulness of this method is suspect, and because of the inability to obtain backgrounds for P3DDT by this method, it has not been implementable here. In order to put some constraints on the selection of backgrounds for this study, some considerations have been made. Structure factor modeling studies of the crystal fraction for this material have provided evidence regarding acceptable crystalline and amorphous scattering fractions [102]. Additionally, the known existence of the type-II structural phase has provided for the inclusion of the narrower features in the background profile [93].

The first five ($h00$) Bragg reflections, before the application of any corrections, are plotted in Fig. 4.41 (note that the intensities are plotted on a log_{10} scale). The arrows indicate the location of background peaks that originate from the type-II, secondary structural phase. Even though the existence of these "background" peaks is assured, their removal from the type-I peak profiles of interest was not a trivial exercise. The first order peak of the background spectra is located safely between the (100) and (200) peaks, making its removal straightforward, but the second and third order type-II peaks are located intimately near or underneath the (300) and (400) type-I peak profiles. In fact, the second order background peak (indicated by the arrow at $\sim 9^\circ\ 2\theta$) starts out on the low angle shoulder of the (300) peak at 10°C and slowly makes its way, relatively, to higher angle, until it has nearly the same scattering angle as the (300) peak, at 60°C. This fact strongly inhibits the ability to unambiguously determine the peak profile of the (300) peak in this temperature range.

The presence of multiple, resolvable ($h00$) reflections both lessens the potential impact that an inaccurate peak profile imparts on final disorder parameter values, and provides clues to the experimenter regarding the correct peak profile by considering the progression of peak profiles as a function of order and temperature. This consideration allows the experimenter to choose an "arbitrary" background profile and iteratively make small, reasonable changes such that the resulting ($h00$) peak profiles follow a monotonic progression of peak shapes as a function of order and temperature. Additional importance in accurately resolving the (300) peak originates from uncertainties involved in the "shadowing" corrections applied to the most intense (100) peak. Naively, this expected functionality of peak with order resulting from equations (4.24) and

(4.25), allows one to confidently and reliably choose an appropriate background, but few authors have commented on deviations from expected linear relationship between peak shape and peak order correlations, and only two studies of polymer systems have been completed that have three [130] or more [131] orders of a family of reflections. When the above procedure is not implemented to obtain a "correct" (300) peak profile, the resulting crystal size and disorder parameters can become erroneously large, while lattice parameter fluctuation become almost nonexistent.

The difficulty involved in subtracting type-II background effects from peak profiles is not present at higher temperatures. As temperatures reach above the LC transition temperature, the secondary phase disappears, and the subtraction of the background is no longer ambagious.

The presence of five orders of reflection also gives some insight into the potential problems present in studies involving material possessing only a small number of reflection orders. When applying the Warren-Averbach/Crist-Howard method to P3DDT diffraction spectra using only the first two orders of reflection, the separation of size and fluctuation effects is trivial (two points make an unambiguous line). However, when more than two orders of reflection are considered, two equations are available for separating the size and fluctuation coefficients, namely equations (4.24) and (4.27). When fluctuations are small, both should yield similar results, yet in this study both do not necessarily give the similar results. Fig. 4.42 shows the functionality of Fourier coefficients verses the square of the order h for temperatures of 30°C and 80°C. For the 30°C sample, the coefficients appear to be relatively linear for the first 9 coefficients, especially when one considers that the error bars for the 4^{th} order peak are large.

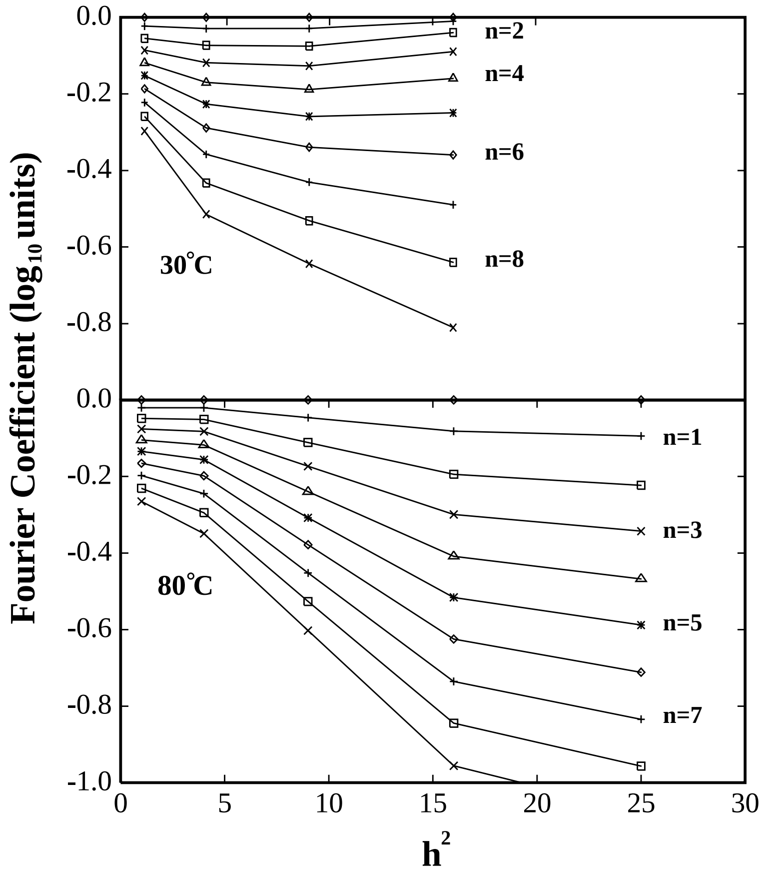

Figure 4.42: P3DDT Fourier cosine coefficients for the first four to five orders of the $(h00)$ reflection vs h^2 for temperatures of 30°C (top) and 80°C (bottom).

Deviations from the linearity in Fig. 4.42 imply that either the approximations in equation (4.24) have failed, or possibly that errors in background subtraction have occurred.

Fig. 4.43 and Table 4.4 show qualitatively the functional dependence of the peak FWHM and peak shape as a function of temperature and order. There does not appear to be any consistent, functional dependence of peak width verses order, neither is there a consistency of Gauss/Lorentz character of peak shape. In fact, the shape of the peaks tend to change from a slightly Gaussian character with an average $\eta = .54$ for the first order reflection to a predominantly Lorentzian character for the fourth order peak and a predominantly Gaussian character for the second order peak. From a crude Debye-Scherrer analysis of the first order peak, one would describe the narrowing of peak width from an increase in crystallite size from 270Å to 310Å (see the top of the middle of Fig. 4.46).

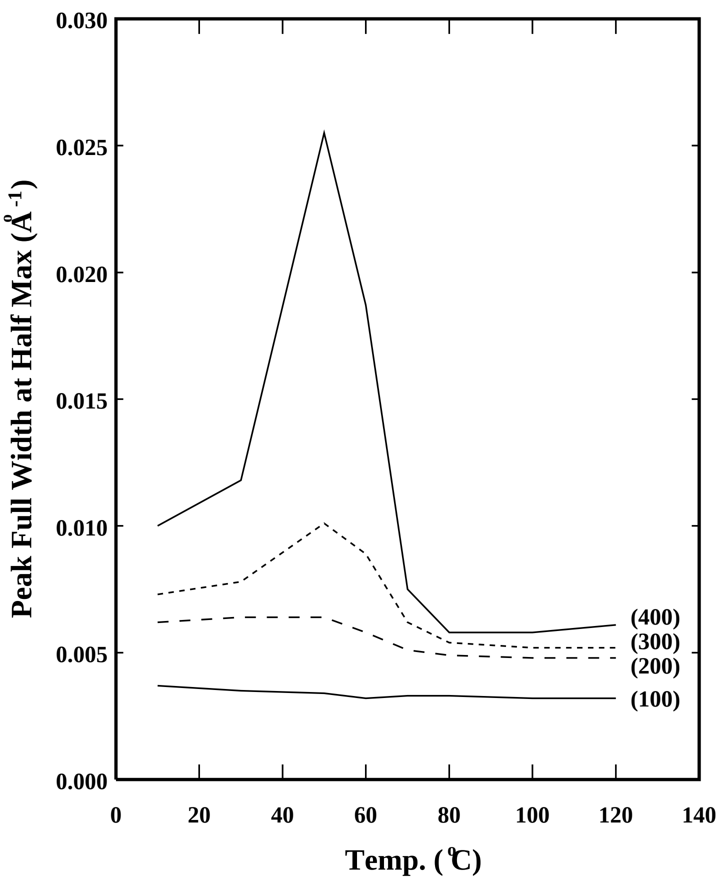

Figure 4.43: A plot of the variations in peak width, indicative of the "Debye-Scherrer" crystal size, for each indicated ($h00$) reflection.

Qualitatively, the spectrum for temperatures below the LC point, between 60°C and 70°C, behave like the 30°C plot (for this temperature range, the error

Table 4.4: Table of η and Debye-Scherrer peak widths.

Temp.	$h = 1$		$h = 2$		$h = 3$		$h = 4$	
($^\circ C$)	η	width(Å)	η	width(Å)	η	width(Å)	η	width(Å)
10	0.60	271.	0.77	160.	0.83	140.	0.63	117.
30	0.61	287.	0.74	161.	0.81	132.	1.00	107.
50	0.61	291.	0.16	152.	0.33	106.	0.38	45.
60	0.58	308.	0.10	174.	0.30	124.	0.06	51.
70	0.58	306.	0.63	196.	0.25	161.	0.84	140.
80	0.64	301.	0.78	202.	0.45	184.	0.02	159.
100	0.59	311.	0.64	210.	0.45	193.	0.36	178.
120	0.62	310.	0.57	210.	0.45	193.	0.00	173.

bars on the 4^{th} order peak are large), and those above the LC point have trends that are difficult to interpret like the 80°C plot (error bars on the 4^{th} order peak are more reasonable in this temperature range with the 5^{th} order peak defined well enough to use) (see bottom of Fig. 4.42).

4.4 Results and Discussion

Separating size and distortion according to (4.24) results in size coefficients with little or no "hook effect", and the resulting plot of $f(n)$ verses n, shown in Fig. 4.44, results in a linear relationship (except for the expected lowest order coefficients) making separation of g and e straightforward and unambiguous. However, when the (300) peak is taken into consideration, a plot of $\ln[A_h(n)]$ verses h^2 quite frequently appears nonlinear and/or nondecreasing (see Fig. 4.42), which is consistent with studies of other materials [114,130,131]. When higher order peaks are considered, the break from nonlinearity is further magnified. This suggests that the approximations used in (4.24) and (4.27) may be breaking down by the 3^{rd} order reflection or sooner, and/or higher moments of Z_h may be important. Fitting the first three orders with equation (4.24) had little effect on N_3, but had larger effects on the values of e and g.

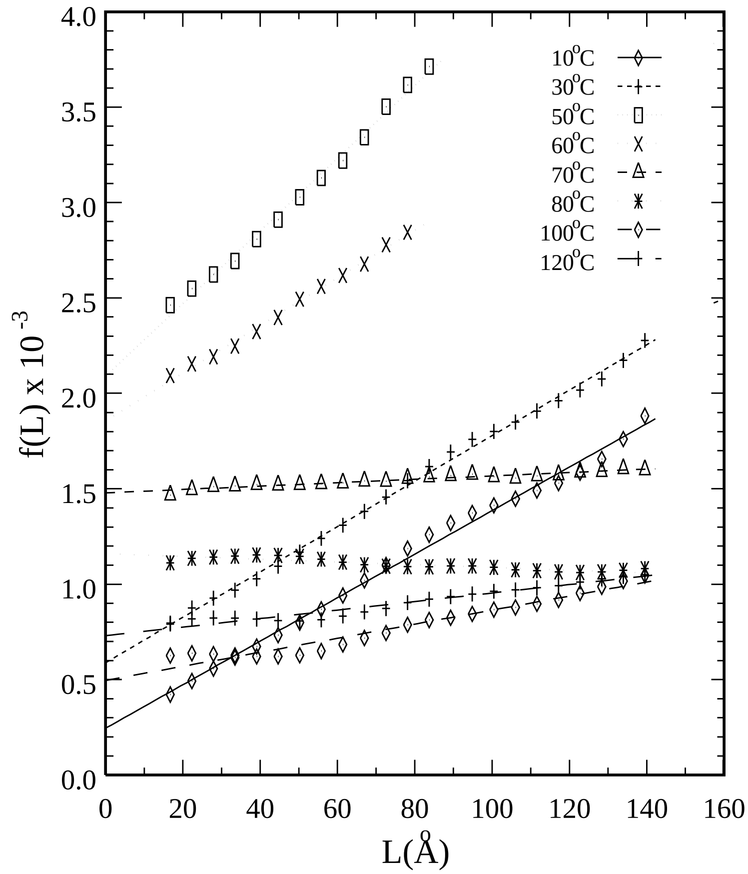

Figure 4.44: Plot of f(L) verses L as obtained from equation 4.24. The negative slope and intercept give $<e^2>$ and $<g^2>$ respectively.

Using the alternate method, by fitting the data to equation (4.27), produces a better multiorder fit, but that is to be expected with the use an extra fitting parameter. Although this method produces similar size coefficients as the above method, most temperatures give comparatively, smaller values of e and g, while at the other temperatures the values of e and g are undetermined because plots of $f(n)$ verses n, shown in Fig. 4.45, posses either a significant negative slope or negative y-intercept.

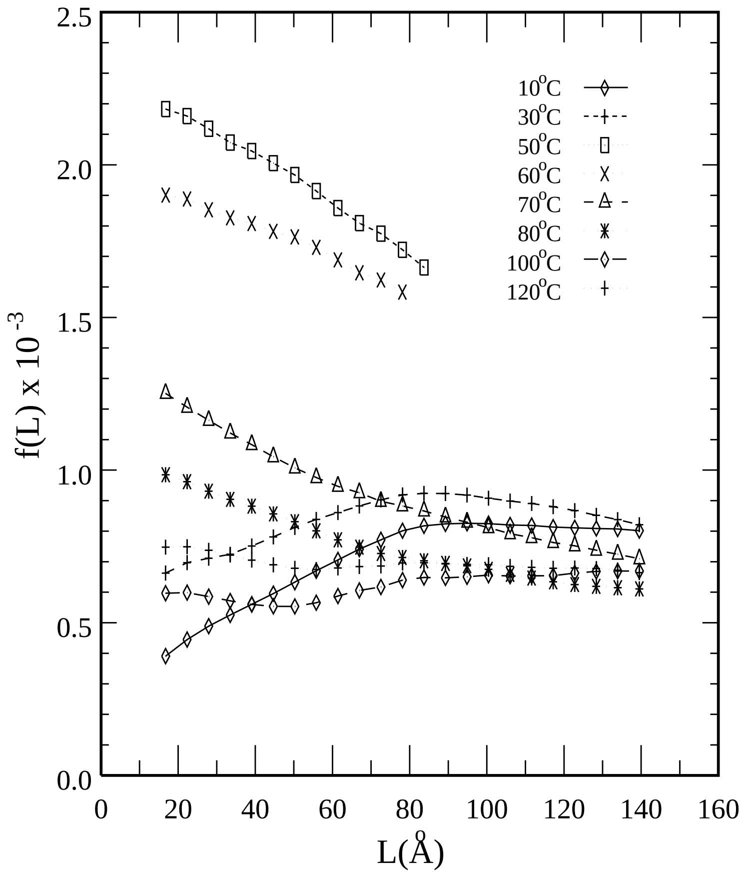

Figure 4.45: Plot of f(L) verses L as obtained from equation 4.27. The negative slope and intercept give $<e^2>$ and $<g^2>$ respectively.

The narrowing of observed (100) peak width as a function of temperature, to first order, has been attributed to an increase in crystal domain size [89] without taking other broadening mechanisms into consideration, and in the case of P3DDT, this proves be a misleading assumption. It is very likely that this assumption has led to misinterpreted "annealing" in other polymer systems, leading to proposed procedures that may not increase crystal size as much as reduce intrinsic disorder, resulting in variations of disorder parameters that reflect changes in structural homogeneity.

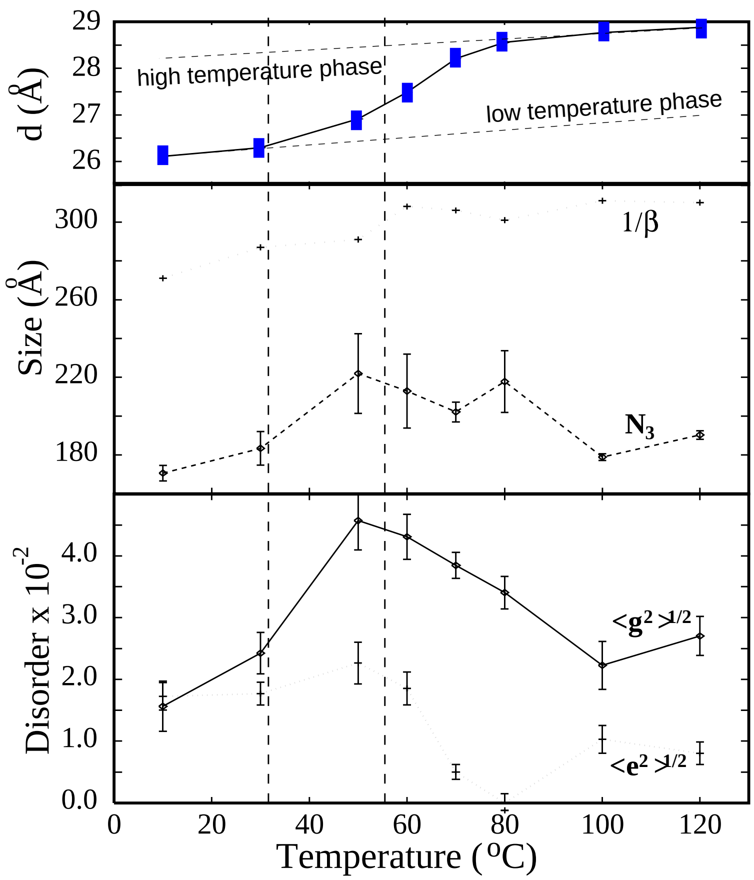

Figure 4.46: Plots of various parameters as a function of temperature top to bottom: interlamellar d-spacing, "Debye-Scherrer" crystal size, volume weighted crystal size, displacement disorder, and lattice parameter fluctuation.

When instrumental broadening effects are taken into account, the Debye-Scherrer average crystal size of 270Å, at room temperature, is not consistent with the value of 170Å when disorder effects are taken into account. In fact, when the thermal expansion of the polymer unit cell is taken into account, a Debye-Scherrer analysis indicates that the average crystallite size remains

Table 4.5: Peak Profile Analysis Results

Temp($^\circ C$)	d(Å)	N_3(Å)	g	e
10	26.1	171.	0.016	0.017
30	26.3	183.	0.024	0.018
50	26.9	222.	0.046	0.023
60	27.5	213.	0.043	0.019
70	28.2	202.	0.038	0.005
80	28.6	218.	0.034	0.000
100	28.8	179.	0.022	0.010
120	28.9	190.	0.027	0.008

relatively constant as a function of temperature at 10.5 unit cells. Meanwhile, peak profile analysis discovers that the modest narrowing of the (100) peak from 10°C to 50°C is attributed to a possible increase in crystal size from 6.5-7.5 unit cells and a decrease in disorder of the second kind with the lattice parameter fluctuation increase paralleling the average crystal size. Between 50°C and 80°C the peak widths narrow sharply even though the calculated "crystal size" shows only a modest reduction to 6.5-7 unit cells. At 120°C, immediately below the isotropic melting temperature, the observed crystal size is 6.5 unit cells or 190Å even though the average crystal size is modestly larger, the reduction in lattice parameter fluctuation and disorder provides narrower peaks as a function of order, making these peaks easily discernable from the background.

A simple first order transition picture that might explain the observance of the variation of peak width as a function of order and temperature would yield a picture in which individual crystallites would sequentially melt yielding, in the case of a heterogeneous system, a two-phase coexistence of the high temperature

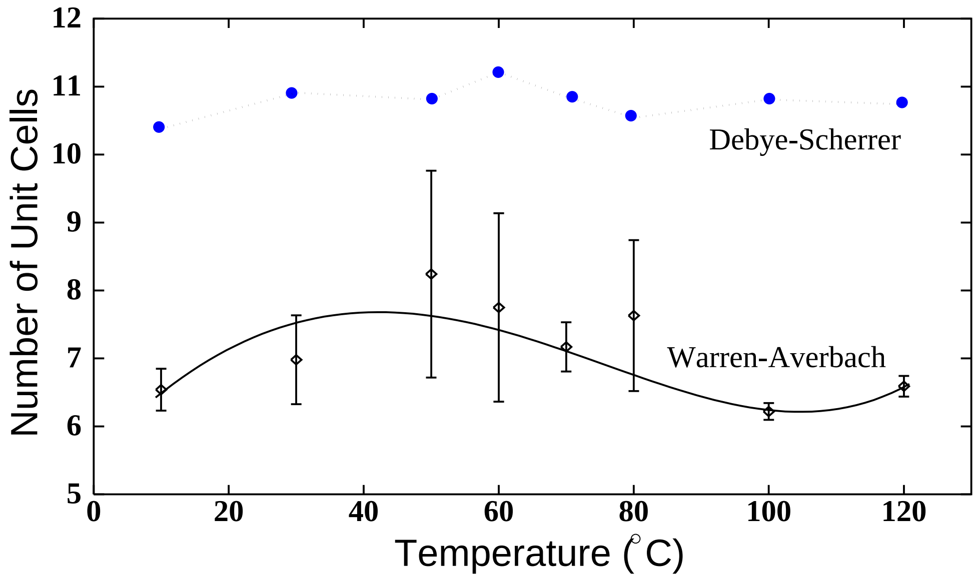

Figure 4.47: Plot of the average number of unit cells contained in a crystallite as determined by Debye-Scherrer (top) and Warren-Averbach (bottom).

and low temperature phases over an extended temperature range. Thus the scattering profiles would be represented by a superposition of monotonically increasing/decreasing contributions of the two phase fractions possessing two different thermal expansion rates (see the top of Fig. 4.46).

However the experimental data is clearly in contradiction with this theorized scenario. In all cases, a *single* well-defined set of multiple higher order peaks is recorded. More important is the functional variation in the peak intensities and peak widths on cycling through the phase transition. Thus, there appears to be a localized, uncorrelated melting of the side chains within each and every P3DDT crystallite. These local inhomogeneities play the role of "defects" and, as such, would be expected to generate an extremely strong signature indicative of fluctuation disorder. The process is probably rather general in lamellar systems but we are unaware of any prior attempts to obtain a rigorous result.

4.5 Conclusions

Peak profile analysis has not been utilized extensively in the pursuit of understanding the role that disorder plays in polymer structure. The lack of available structural probes able to uncover microstructure at this length scale suggests more frequent use of this type of analysis. Although the topic of paracrystallinity and disorder, in these less perfectly ordered systems, has been extensively discussed in theory, many discrepancies between theory and practice seem to exist. The inability to obtain, independent "amorphous" background profiles for consequent peak profile determination does lend some doubt as to the reliability of this technique on semicrystalline polymers, yet this study has shown that these difficulties can be overcome when suitable conditions exist.

P3DDT remains an interesting candidate for the application of peak profile analysis because of the large number of identifiable orders of the $(h00)$ reflections, yet it still possess all the other drawbacks. By considering spectra at various temperatures, both below and above a known LC transition, many of these complications have been minimized. The consideration of multiple spectra and the requirement that iterative changes in background profile do not change significantly, has provided for a reliable method for deconvolving the various causes of line profile broadening, and has led to some sucess here.

The Fourier analysis of multiple peak profiles provides the most objective procedure for separating the major peak broadening mechanisms, namely the effects of crystal size and disorder. This analysis has shown that crystal size, lattice parameter fluctuation, and displacement disorder of the second kind are all important factors in the peak shape of P3DDT. Nevertheless, more studies on similar polymer systems need to be done to see if other materials exhibit analogous variations in these parameters. Obvious candidates are side chain substituted materials, similar to P3DDT, that have increased side chain crystallinity. These large d-spacings provide for multiple peak profiles that are relatively easy to distinguish from the amorphous background.

This peak profile analysis has revealed much about the variation of crystal size, lattice parameter fluctuation, and displacement disorder within P3DDT as a function of temperature. The overestimation of crystal size by Debye-Scherrer methodology has been demonstrated, with changes in crystal size being best described as a thermal expansion of the 6.5 unit cell, average crystallite dimension, with little or no real change in crystal size. Lattice parameter fluctuation has been shown to lower significantly through the LC phase transition from a value near 2% to a value below 1%. Although this has observable consequences in peak narrowing, the variations in displacement disorder have equivalent influences on observed peak profiles. Finally, displacement disorder has been shown to peak around the LC phase transition revealing an inhomogeneous structural phase transition. Starting out with minimum displacement disorder of 1.5% for 10°C, having a maximum of 4% at 55°C near the LC transition, and approaching another local minimum of 2.5% before melting near 120°C, these fluctuations in displacement disorder suggest that local structural inhomogeneities are observed as "defects".